Measurement of inelastic electron impact on ozone: Absolute differential cross sections for excitation of the Hartley band

Christopher J. Sweeney and Tong W. Shyn
Space Physics Research Laboratory, University of Michigan, Ann Arbor, Michigan 48109-2143
(Received 23 October 1995)

By means of a crossed-beam technique, we have conducted absolute differential cross-section measurements for the excitation of ozone's Hartley band by electron impact. The angular range covered was from 12° to 156°, while the impact energies employed were 7, 10, 15, and 20 eV. The angular distributions indicate that the Hartley band has a composite nature, arising from at least one optically allowed and at least one optically forbidden transition. Candidates for these transitions are indicated with help from the results of theoretical calculations. Unfortunately, aside from the well known $1\ ^1B_2 \leftarrow X\ ^1A_1$ allowed transition observed in optical spectra, definitive assignments for these transitions cannot yet be made. Integrated cross sections were calculated from the measured differential cross sections. The former exhibit a maximum near 15-eV impact.

PACS number(s): 34.80.Gs

I. INTRODUCTION

When considering the prognosis for the Earth's environment, perhaps the first issue which comes into most people's minds is the destruction of the ozone layer. Given ozone's importance in attenuating lethal solar ultraviolet radiation and in determining the progress of chemical reactions within the atmosphere, this is hardly surprising. To gain a proper understanding of the fundamental nature of this molecule and of its roles in these processes, numerous investigations of ozone have been undertaken. As a result, we now have a fairly complete knowledge of ozone's photoabsorption spectrum [1,2]. While our understanding of the quantum-mechanical structure of ozone [3–11], its atmospheric abundance [12], and its environmental roles [13,14] is perhaps not quite as complete, substantial progress is also being made on all three of these fronts.

Not much electron scattering research has been conducted on ozone, however. Theoretical investigations here are limited to a few elastic scattering calculations [15–17], while experimental investigations are restricted to a couple observations of ozone's electronic-state excitation by electron impact [18,19], an electron-impact ionization study [20], an oscillator strength measurement [21], a measurement of absolute differential elastic scattering cross sections [22], and a measurement of absolute differential vibrational-excitation cross sections [23]. This dearth of information is curious, as transitions incited by electron impact are not subject to the stringent optical selection rules. Optically allowed transitions manifest themselves in the small-angle scattering of electrons at high impact energies, while optically-forbidden transitions dominate near threshold excitation energy and at large electron scattering angles [24,25]. Electron-impact investigations thus give insight into forbidden transitions not otherwise available, and complement traditional photabsorption spectroscopy in providing information vital to the understanding of atomic and molecular structure and dynamics.

In this article, we will begin to remedy the paucity of data for the electron-ozone collision system. Here we shall present results of measurements of absolute differential cross sections for the excitation of ozone's Hartley band by electron impact. Lying between about 4 and 6 eV in excitation energy, this band is the one most crucial for the filtering of ultraviolet radiation in the atmosphere. Furthermore, its excitation results in the dissociation of ozone into chemically reactive atomic and molecular oxygen fragments. Our experiments were conducted by means of a crossed-beam technique, and covered scattering angles from 12° to 156°, in 12° increments. The impact energies we employed were 7, 10, 15, and 20 eV. The angular character of the cross sections indicates the presence of at least one forbidden transition, in addition to the well known $1\ ^1B_2 \leftarrow X\ ^1A_1$ allowed transition present in optical spectra. Other allowed transitions may also be present. A definitive assignment of these remaining transitions cannot yet be made, but we will provide some possibilities for their nature with help from the results of theoretical calculations. Integrated-excitation cross sections were computed from the measured differential-excitation cross sections, and exhibit a maximum near 15-eV impact.

II. EXPERIMENT

The majority of our apparatus and the experimental procedures we employ in electron-atom and electron-molecule collision investigations have been described in detail elsewhere in the physics literature [22,26–28], so we will here provide only a brief account of them.

Our apparatus contains three principal subsystems: an ozone production and storage system–neutral-ozone-beam source, a monoenergetic-electron-beam source, and a scattered-electron detector. All three are housed in a vacuum system divided into two chambers—upper and lower—which are pumped differentially. This vacuum system is surrounded by three sets of mutually perpendicular Helmholtz coils which attenuate unwanted magnetic fields, including the Earth's. We have measured the net magnetic field in the electron-molecule interaction region to be less than 20 mG in any direction. Since this interaction region is located about 10 cm from our scattered-electron detector, the maximum

angular deviation imparted by magnetic fields to the trajectory of a 1 eV electron in our apparatus is less than 2°.

For the production of ozone, we pass extra-dry grade molecular oxygen near atmospheric pressure through a 12000 VAC, 60 Hz discharge tube. The gas mixture leaving this tube is composed of perhaps 5% ozone, the balance being molecular oxygen. Ozone is concentrated and stored by passing this mixture through a 300 cc bottle fabricated from No. 304*L* stainless steel, filled with about 250 cc of silica gel, and maintained at dry-ice temperatures (about 195 K). At these temperatures, the silica gel selectively absorbs the ozone; the remaining molecular oxygen is removed by a two-stage mechanical pump. ''Charging'' the silica gel overnight in this fashion provides enough ozone for at least eight hours of experimentation the next day. Note that with this method of ozone storage we avoid having to contend with extremely explosive liquid ozone.

To release the ozone into our vacuum system, we simply remove the storage bottle from the dry ice. The flow rate of ozone from the bottle is regulated by a needle valve, and the ozone is transported to the vacuum system via tubing formed from teflon. Fiberglass batting is present at the exit of the bottle to prevent the escape of any silica gel into the teflon tubing under the influence of pressure gradients. The teflon tubing ends at a teflon double skimmer located at the junction between the upper and lower chambers. This skimmer provides a collimated neutral-ozone beam directly vertically downward into the lower chamber where the electron-ozone collisions occur.

By comparison of the energy-loss spectra produced with this beam with known energy-loss spectra for the low-lying electronic and vibrational state excitations of molecular oxygen [29,30], we estimate our ozone source to be of greater than 95% purity. This obviates the removal of any molecular oxygen background contributions during data analysis. The two key ingredients in maintaining the high purity of ozone appear to be the use of almost atmospheric pressure flow during the charging of the silica gel with ozone, and the use of only relatively inert materials such as teflon, No. 304*L* stainless steel, No. 316*L* stainless steel, and glass for construction.

The electron-beam source is located near the central axis of the lower chamber and is rotatable continuously from $-90°$ to 160°. Comprising it are an electron gun based on a thoria-coated iridium filament, a 127° cylindrical energy selector, two electron lenses, and both vertical and horizontal electron-beam deflectors. The electron beam which emerges from this source has a current exceeding 10^{-8} A and an angular divergence of no more than 3° full width at half maximum (FWHM). The mean energy of the electrons in this beam is calibrated via the 19.35-eV resonance of helium.

Fixed to the lower chamber's wall is the scattered-electron detector. It is located in a horizontal plane with the electron-beam source. The detector is composed of 127° cylindrical and hemispherical energy analyzers in tandem, two electron lens systems, and a Channeltron electron multiplier. The response profile of the combined electron beam-source–scattered-electron detector is the convolution of the true energy profile of the electron beam with the response profile of the detector. This resulting net response is Gaussian in form,

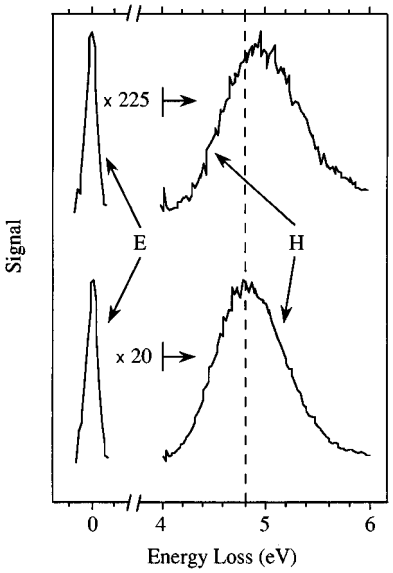

FIG. 1. Two typical raw electron energy-loss spectra for the Hartley band of ozone. The impact energy for both was 10 eV. The lower spectrum was for a scattering angle of 12°—which favors allowed transitions—while the upper was for a scattering angle of 156°—which favors forbidden transitions. The elastic scattering peaks are labeled ''*E*,'' while the Hartley excitation bands are labeled ''*H*.'' The elastic peaks of both spectra were arbitrarily scaled to the same magnitude, for ease of viewing. To magnify the Hartley bands to the same peak intensity as the elastic peaks required separate changes of scale on the right, as the figure indicates. The vertical dashed line shows the slight shifting of the Hartley band's peak intensity as the scattering angle changes. While subtle, this effect was consistently present in our data at all impact energies, and indicates the presence of both allowed and forbidden transitions, as discussed in the text.

and for the present measurements was set to about 80-meV FWHM.

During our measurements, the mean energy of the electron beam is maintained at a constant value, while the electron detector's energy acceptance window is swept over both the elastic scattering region, and the energy-loss region corresponding to excitation of the Hartley band. Data are accumulated and stored by a microcomputer running locally developed software. This process is repeated over the prescribed set of scattering angles and impact energies. The results are spectra like those shown in Fig. 1. The lower spectrum in this figure is for 10-eV impact and a scattering angle of 12°, while the upper one is for the same impact energy, but a scattering angle of 156°. The narrow peaks at the left in both the upper and lower spectra correspond to elastic scattering, while the broad bands near the centers of both correspond to excitation of the Hartley band.

III. DATA ANALYSIS

To calculate absolute differential-excitation cross sections, we first corrected our measured energy-loss spectra for the effect of detector efficiency. This involved measuring the elastic scattering signal strengths for pure molecular oxygen at various energies over the region of interest. By comparing the signal strengths with the elastic cross sections measured

TABLE I. Uncertainties (in %) in the Hartley band measurements.

Source of uncertainty \ E (eV)	7 and 10	15 and 20
Raw data	±5	±7
Detector efficiency	±20	±15
Elastic cross sections	±15	±15
Total	±26	±22

previously by one of the present investigators and a collaborator [31], we established a polynomial form for the relative efficiency of our apparatus at detecting scattered electrons with respect to the electrons' energies. This polynomial was then used to adjust the raw energy-loss spectra of ozone to properly reflect the detector's nonconstant efficiency with respect to energy.

Noting that cross sections scale as the areas under the excitation peaks, we next calculated relative elastic and Hartley band excitation cross sections by integrating these areas numerically via the trapezoid rule. These relative cross sections were placed on the absolute scale by normalization to the absolute elastic cross sections of ozone which we measured previously [22].

Integrated cross sections were generated by numerically integrating the differential cross sections, again by the trapezoid rule. This required that we extrapolate our differential cross sections to both 0° and 180°, which we did in a semi-exponential fashion. Due to the smallness of the factor $\sin\theta$ in the integrand at these extreme forward and backward angles, the error introduced into the integrated cross sections by these extrapolations is negligible.

All uncertainties in our measurements were essentially uncorrelated and were therefore added in quadrature to determine the net uncertainty of the cross sections. The sources of uncertainty and their values, along with the cross sections' net uncertainties, are listed in Table I.

IV. DISCUSSION OF RESULTS

As we stated earlier, the angular character of electron-impact cross sections indicates the presence of allowed or forbidden transitions in a given excitation. The presence of both types of transition is apparent in the Hartley band over the incident energy range we employed. This is demonstrated by the absolute numerical values for the cross sections listed in Table II, the energy-loss spectra given by Fig. 1, and the cross sections' graphical depictions provided by Figs. 2, 3, and 4.

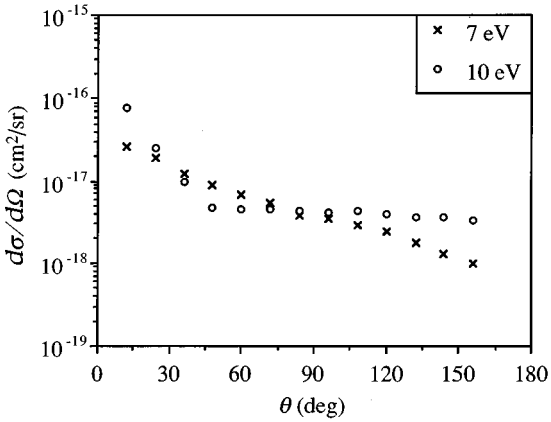

FIG. 2. Absolute differential cross sections for excitation of the Hartley band of ozone by electron impact. The impact energies portrayed in this figure are 7 and 10 eV.

As demonstrated in Fig. 1, the peak energy of the Hartley band's excitation line shape changes slightly as the scattering angle is changed from 12° to 156°. This change is due to the different mixtures of allowed and forbidden transitions at the different angles, the former being more prominent at the lower angles and the latter being more prominent at the higher angles. (Note that while Fig. 1 is for 10-eV impact, similar trends were apparent at the other impact energies.)

Figure 2 shows the differential cross sections at 7- and 10-eV impact. The 7-eV results vary by less than two orders of magnitude over the angular range considered. We see also that the cross sections here lack any pronounced forward peak and decrease in magnitude relatively gradually as the scattering angle increases. The lack of strong forward scattering indicates the substantial presence of forbidden transitions at this energy, in addition to allowed transitions. Our 10-eV results have a somewhat different character. While the differential cross sections here again vary by less than two orders of magnitude, this time they exhibit much stronger forward scattering accompanied by relatively isotropic scattering at middle and high angles. Such angular character indicates that at this energy allowed transitions play a much greater role, although forbidden transitions are still present in significant amounts. The more minor role played by forbidden transitions at 10-eV impact is to be expected, as we are now farther from the excitation threshold. The differential cross sections at 15- and 20-eV impact are shown in Fig. 3.

TABLE II. Absolute cross sections for the excitation of the Hartley band of ozone by electron impact. Units for the differential cross sections are 10^{-18} cm^2/sr, while those for the integrated cross sections are 10^{-18} cm^2. Parentheses enclose extrapolated values.

	θ (deg)														
E (eV)	12	24	36	48	60	72	84	96	108	120	132	144	156	168	σ_i
7	26	19	12	8.9	6.7	5.4	3.8	3.5	2.9	2.4	1.8	1.3	0.97	(0.70)	69
10	78	25	9.9	4.7	4.5	4.6	4.4	4.2	4.3	3.9	3.7	3.6	3.4	(3.0)	88
15	100	42	11	4.4	4.1	3.7	3.9	3.1	2.6	3.1	2.9	2.2	(3.0)	(3.5)	95
20	84	30	2.8	1.2	1.5	1.7	1.7	1.4	1.3	1.2	1.6	2.7	(3.5)	(5.0)	60

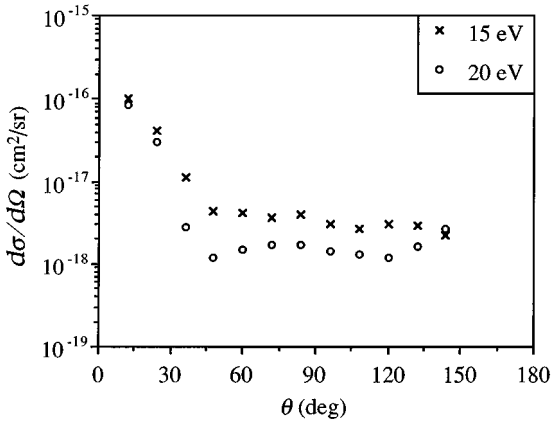

FIG. 3. Absolute differential cross sections for excitation of the Hartley band of ozone by electron impact. The impact energies portrayed in this figure are 15 and 20 eV.

At both energies the cross sections have an angular character very similar to that at 10-eV impact, suggesting very nearly the same mixture of allowed and forbidden transitions. At 20-eV impact, however, the cross sections exhibit a hint of D-wave character. Integrated cross sections are displayed in Fig. 4. They exhibit a maximum near 15-eV impact.

At all energies, the principal transition in the spectra is the $1\,^1B_2 \leftarrow X\,^1A_1$ allowed transition familiar from photoabsorption. This transition has a peak vertical excitation energy consistently determined by experimentalists to be between 4.85 and 4.89 eV [21], and arises predominantly from the promotion of a $1a_2$ electron to the $2b_1$ orbital, with only minor contributions from the $2b_1^2 \leftarrow 1b_1 1a_2$ electronic configuration change [11]. The transition's excitation line shape results from excitation of ozone's symmetric stretching and bending vibrational mode progressions, with dissociation via the asymmetric stretching mode progression to $O(^1D) + O_2(a\,^1\Delta_g)$ causing the broadening of the bands into a continuum [21,32].

An identification of the remaining components of the Hartley band cannot be definitively made at this time, as the available theoretical predictions of ozone's vertical state excitation energies frequently disagree, and there have not yet been any theoretical predictions of the detailed nature of the angular distributions corresponding to excitation of these states. There is some consensus, however, about which states' vertical excitation energies lie within the proximity of the $1\,^1B_2$ state's, even though the predictions for this latter state often disagree with the accepted experimental value by more than 1 eV. These appear to be the $2\,^3A_1$ and $2\,^3B_2$ states, whose excitations are forbidden. This situation is summarized in detail in Refs. [11] and [21]. Using a minimal basis set-generalized valence bond, generalized valence bond-configuration interaction, and polarization-configuation interaction techniques, for instance, Hay, Dunning, and Goddard consistently predicted the $2\,^3A_1$ and $2\,^3B_2$ states to have vertical excitation energies within 1 eV above the $1\,^1B_2$ state's [3]. Messmer and Salahub, employing the self-consistent-field-X_α–scattered-wave method, obtained a value for the $1\,^1B_2$ state's vertical excitation energy nearly 2 eV below the accepted experimental value, but also posited the location of the $2\,^3A_1$ and $2\,^3B_2$ states to be within 1 eV of the $1\,^1B_2$ state as regards vertical excitation energy [4]. Thunemann, Peyerimhoff, and Buenker obtained what is perhaps the most accurate vertical excitation energy for the $1\,^1B_2$ state, using multireference-configuration interaction methods, at 4.97 eV, and predicted the states $2\,^3A_1$ and $2\,^3B_2$ states to have vertical excitation energies within 1.5 eV above this value [6]. A similar trend is reflected in the multiconfiguration interaction self-consistent field and multiconfiguration linear response calculations of Nordfors, Ågren, and Jensen, who found the $1\,^1B_2$ state at a vertical excitation energy within 0.1 eV of the accepted experimental value, and the $2\,^3A_1$ and $2\,^3B_2$ states vertically within about 0.5 eV of the predicted value for $1\,^1B_2$ [10]. Most recently, Banichevich and Peyerimhoff obtained, by means of multireference-configuration interaction methods, a vertical excitation energy of 5.16 eV for the $1\,^1B_2$ state, and excitation energies for the $2\,^3A_1$ and $2\,^3B_2$ states within 1 eV above this [11]. The consistent findings of these two triplet states just above the $1\,^1B_2$ state suggests that transitions to one or possibly both the former states comprises the forbidden component of the Hartley band which we have observed by electron impact. We must reemphasize, however, that plausible as this interpretation may be, it is only speculative.

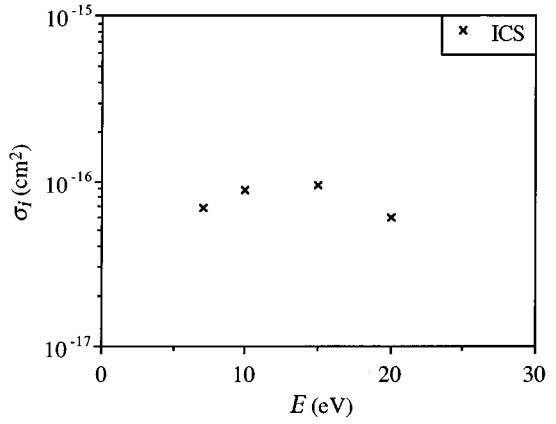

FIG. 4. Absolute integrated cross sections (denoted "ICS") for excitation of the Hartley band of ozone by electron impact.

V. CONCLUSION

By means of a crossed-beam method, we have measured absolute differential cross sections for the excitation of the Hartley band of ozone by electron impact. The scattering angles considered were 12°–156° in 12° increments, while the impact energies used were 7, 10, 15, and 20 eV. The angular behavior of the cross sections indicates the presence of at least one forbidden transition, in addition to the well known $1\,^1B_2 \leftarrow X\,^1A_1$ allowed transition apparent in optical spectra. Other allowed transitions may also be present. The identities of the forbidden transitions cannot be clearly established as this time, but as we have disscused, the most appealing candidates appear to be the $2\,^3B_1 \leftarrow X\,^1A_1$ and $2\,^3A_2 \leftarrow X\,^1A_1$ transitions. Integrated cross sections were calculated from the measured differential cross sections; the former exhibit a maximum near 15-eV impact.

ACKNOWLEDGMENTS

The authors are grateful for support provided for this research by the National Science Foundation, under Grant No. ATM-9415678. In addition, we are indebted to Scott G. Edgington, Professor J. W. Rasul, and Beth Weinberg for valuable conversations regarding ozone.

[1] J. I. Steinfeld, S. M. Adler-Golden, and J. W. Gallagher, J. Phys. Chem. Ref. Data **16**, 911 (1987).
[2] J.-M. Flaud, C. Camy-Peyret, C. P. Rinsland, M. A. H. Smith, and V. M. Devi, *Atlas of Ozone Spectral Parameters from Microwave to Medium Infrared* (Academic Press, Boston, 1990).
[3] P. J. Hay, T. H. Dunning, Jr., and W. A. Goddard III, J. Chem. Phys. **62**, 3912 (1975).
[4] R. P. Messmer and D. R. Salahub, J. Chem. Phys. **65**, 779 (1976).
[5] P. J. Hay and T. H. Dunning, Jr., J. Chem. Phys. **67**, 2290 (1977).
[6] K. H. Thunemann, S. D. Peyerimhoff, and R. J. Buenker, J. Molec. Spectrosc. **70**, 432 (1978).
[7] N. Padial, G. Csanak, B. V. McKoy, and P. W. Langhoff, J. Chem. Phys. **74**, 4581 (1981).
[8] R. O. Jones, J. Chem. Phys. **82**, 325 (1985).
[9] M. Braunstein, P. J. Hay, R. L. Martin, and R. T. Pack, J. Chem. Phys. **95**, 8239 (1991).
[10] D. Nordfors, H. Ågren, and H. Jensen, Int. J. Quantum Chem. **40**, 475 (1991).
[11] A. Banichevich and S. D. Peyerimhoff, Chem. Phys. **174**, 93 (1993).
[12] Global ozone research and monitoring project, in *Scientific Assessment of Ozone Depletion: 1991*, Report No. 25 (World Meteorological Association, Geneva, 1991).
[13] R. P. Wayne, Atmos. Environ. **21**, 1683 (1987).
[14] R. P. Wayne, in *Handbook of Environmental Chemistry*, edited by O. Hunzinger (Springer, Berlin, 1989), Vol. 2, Part E.
[15] K. N. Joshipura, Indian J. Pure Appl. Phys. **23**, 525 (1984).
[16] K. N. Joshipura, Pramana J. Phys. **32**, 139 (1989).
[17] Y. Okamoto and Y. Itikawa, Chem. Phys. Lett. **203**, 61 (1993).
[18] R. J. Celotta, S. R. Mielczarek, and C. E. Kuyatt, Chem. Phys. Lett. **24**, 428 (1974).
[19] N. Swanson and R. J. Celotta, Phys. Rev. Lett. **35**, 783 (1975).
[20] M. W. Siegel, Int. J. Mass Spectrom. **44**, 19 (1982).
[21] W. M. Johnstone, N. J. Mason, W. R. Newell, P. Biggs, G. Marston, and R. P. Wayne, J. Phys. B **25**, 3873 (1992).
[22] T. W. Shyn and C. J. Sweeney, Phys. Rev. A **47**, 2919 (1993).
[23] J. A. Davies, W. M. Johnstone, N. J. Mason, P. Biggs, and R. P. Wayne, J. Phys. B **26**, L767 (1993).
[24] S. Trajmar, J. K. Rice, and A. Kuppermann, Adv. Chem. Phys. **13**, 15 (1970).
[25] M. Inokuti, Rev. Mod. Phys. **43**, 297 (1971).
[26] T. W. Shyn and A. Grafe, Phys. Rev. A **46**, 2949 (1992).
[27] T. W. Shyn, C. J. Sweeney, and A. Grafe, Phys. Rev. A **49**, 3680 (1994).
[28] T. W. Shyn, C. J. Sweeney, A. Grafe, and W. E. Sharp, Phys. Rev. A **50**, 4794 (1994).
[29] T. W. Shyn and C. J. Sweeney, Phys. Rev. A **47**, 1006 (1993).
[30] T. W. Shyn and C. J. Sweeney, Phys. Rev. A **48**, 1214 (1993).
[31] T. W. Shyn and W. E. Sharp, Phys. Rev. A **26**, 1369 (1982).
[32] J. A. Joens, J. Chem. Phys. **100**, 3407 (1994).